

# Real-time optimization with persistent parameter adaptation applied to experimental rig

José Matias\* Julio Paez de Castro Oliveira\*\*  
Galo A.C. Le Roux\*\* Johannes Jäschke\*

\* Norwegian University of Science and Technology, Trondheim, Norway

\*\* University of São Paulo, São Paulo, Brazil

**Abstract:** Real-time optimization (RTO) is a steady-state model-based method used for optimizing process operation in chemical plants. The most common implementation, two-step RTO (TS-RTO), updates the steady-state model parameters in the first step, and optimizes this model in the second step. It has a major drawback, which is the need to wait for steady-state. If data from transient periods is directly used for updating the steady-state model parameters, the production optimization results will most likely be sub-optimal, decreasing the benefits. This becomes even more acute if the system is constantly affected by disturbances and has long settling times. Matias and Le Roux [2018] proposed a TS-RTO variant that uses a dynamic estimator to update the steady-state model parameters, which was named real-time optimization with persistent parameter adaptation (ROPA). By using dynamic estimation, it ensures that the model is always updated to the plant and the steady-state optimization can be scheduled at any desired rate without needing to wait for steady-state. This hybrid approach has been successfully tested in simulations. In this paper, we show its first implementation in a lab-scale rig, which emulates a subsea oil well network. The results show that the hybrid approach enables an increase in the optimization frequency and a decrease in the optimization results variability, improving the overall economic performance when compared to the TS-RTO implementation.

*Keywords:* Real-time operating systems, Optimization

## 1 Introduction

Real-time optimization (RTO) is a model-based optimization method applied in operation of industrial processes. The standard approach, also known as two-step RTO (TS-RTO) [Chen and Joseph, 1987], is implemented as two sequential steps. In the first step, the parameters of the system steady-state model are adapted, such that the deviation between its predictions and plant measurements is minimized. In the second step, the updated steady-state model is used in the production optimization problem, in which the system manipulated variables are adjusted for optimizing an economic criterion, like profit, while taking into account operational constraints.

Although used in practice, the TS-RTO has a major drawback, which is the steady-state wait [Câmara et al., 2016]. Since the system is represented by a static model, only steady-state data can be used for parameter updating. Otherwise, the parameters are incorrectly adapted leading to sub-optimal, and potentially dangerous, updates of the manipulated variables. Thus, TS-RTO is triggered only after the plant measurements pass a steady-state detection test. Since, in practice, it is difficult to identify whether data comes from a stationary or transient period [Menezes, 2016], the TS-RTO is not executed often, decreasing its potential economic benefits.

For avoiding the steady-state wait, Matias and Le Roux [2018] proposed replacing the steady-state model adaptation of the TS-RTO by dynamic estimators. This ap-

proach, called Real-Time Optimization with Persistent Parameter Adaptation (ROPA)<sup>1</sup>, avoids the steady-state wait and, thus, allows the plant optimization to be scheduled at any arbitrary rate. Figure 1 compares the TS-RTO and ROPA implementation schemes.

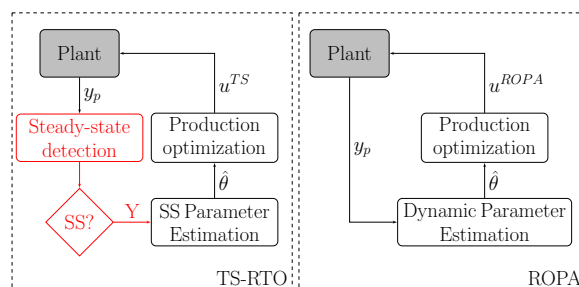


Fig. 1. Comparison between both methods, where:  $u$  are the computed inputs;  $\hat{\theta}$  the estimated parameters, and  $y_p$  the plant measurements.

This new method has been already implemented in simulations and shown promising results. In this paper, we present the first ROPA/Hybrid-RTO implementation, carried out in an experimental rig that emulates a subsea oil well network. The obtained results confirm the previous findings, indicating that ROPA improves the economic performance by increasing the optimization frequency and decreasing the optimization outcomes variability.

<sup>1</sup> The same approach was developed independently by Krishnamoorthy et al. [2018] and called Hybrid-RTO.

## 2 Avoiding the steady-state wait time

The TS-RTO steady-state wait issue has been identified in several papers throughout the years (e.g. Friedman [1995] and Câmara et al. [2016]). Stationary data periods are very difficult to detect [Cao and Rhinehart, 1997], especially for large systems with multiple units interacting with each other [Matias and Le Roux, 2020].

In order to identify the steady-state, statistical methods are applied, e.g.: Student t-test [Kelly and Hedengren, 2013], hypothesis tests using F-statistic [Alekmán, 1994], and R-statistic combined with first-order filters for robustness [Cao and Rhinehart, 1997]. The main problem is that different strategies applied to the same data set yield different results, and the chosen tuning heavily influences the detection outcomes [Menezes, 2016].

One can try to optimally tune these methods [Bhat and Saraf, 2004]. However, in practice, the outcome is usually either too conservative, only few measurements are accepted as steady-state measurements, or too permissive, large periods of clearly transient behavior are indicated as steady-state [Câmara et al., 2016].

Even if the steady-state can be perfectly predicted, there is an inherent delay caused by the TS-RTO parameter estimation step. High disturbance frequencies and/or systems with large response times hinder the start of the optimization cycle.

Alternatively, dynamic optimization methods, like economic model predictive controller [Amrit et al., 2011] can be used. In this case, no steady-state detection is necessary. However, that usually requires changes in the plant decision hierarchy structure and, more importantly, in the mindset of plant operators/engineers.

Based on that scenario, ROPA appears as an interesting alternative, in which the steady-state wait is no longer necessary and no major changes in the plant decision hierarchy are required. Since the parameters are continually estimated, the plant optimization can be scheduled at an arbitrary rate. Note that, even though the parameters are properly updated by the dynamic estimator, using “dynamic” parameters in a steady-state model leads to sub-optimal solutions because the transients are not optimized. Krishnamoorthy et al. [2018] compared the input profiles computed by a dynamic optimization method and by integrating a dynamic estimator with a steady-state optimization method. The authors showed that both profiles are similar as well as the economic results, but the hybrid approach has a much lower computational cost.

## 3 Subsea gas lift oil well network

In subsea oil extraction, the reservoir natural pressure drives the fluids from below the seafloor to the top facilities on the water level. However, in some cases, this pressure is not high enough and artificial lifting methods need to be used. Among them, gas lifting has some advantages, such as a robust design and relatively low cost [Amara, 2017].

In gas lifted systems, compressed gas is injected at the bottom of the well for reducing the fluid bulk density. Consequently, the system hydrostatic pressure in the risers,

which are the vertical connections between the flow lines at seabed and the top facilities, also decreases. Since the risers have lengths up to kilometers, this pressure drop is significant to the system. Thus, by injecting gas into the wells, the back pressure on the reservoir decreases, and the well production increases. On the other hand, if too much gas is injected, the frictional pressure drop effect dominates and the production decreases. Given this scenario, production optimization methods can be a useful tool for finding the optimal injection rate.

An experimental rig was designed to emulate a gas lift oil well network in a small scale. Instead of using oil and gas, the experiments are carried out using water and air. Despite using different fluids, the gas lift effect is still present in the lab rig and, therefore, the production optimization problem can be studied. A simplified flowsheet of the rig is shown in Figure 2. The laboratory setup is divided in three main sections, reservoir, wells and risers:

- The **reservoir** is composed of a 200 L water tank, a centrifugal pump and two control valves. The openings of the valves vary with time and are chosen in order to represent a desired reservoir behavior. With this setting, the reservoir produces only liquid (no gas) and its outflow ranges from 2 to 15 L/min;
- Two parallel flexible pipes with 2 cm inner diameters and length 1.5 m represent the **wells**. Approximately 10 cm after the well “bottom”, air is injected by two air flow controllers, within the range of 1 to 4 sL/min;
- The **riser** section comprises two vertical pipelines. They are inclined with a 90° angle from the wells and their height is 3 m. Such elevation already allows us to see the gas lift effect. On top of the riser, we measure the pressure of each well. The pressure difference between the pump outlet and the separation tank is approximately 0.5 bar. Two valves are located before the separation tank, which are kept fully open during the experiments. For environmental purposes, the liquid is redirected to the reservoir water tank. The air is vented out to the atmosphere.

## 4 Production optimization problem

The optimal economic operation point of the system is found by maximizing the liquid (“oil”) production while penalizing the use of gas lift. The optimization problem also takes into account a given maximum gas lift availability:

$$\begin{aligned} \max_{\mathbf{u}=[Q_{gl,1}, Q_{gl,2}]^T} \quad & J := \alpha_l \sum_{i=1}^2 Q_{l,i} - \alpha_{gl} \sum_{i=1}^2 Q_{gl,i} \\ \text{s. t.} \quad & C := \begin{bmatrix} Q_{gl,1} + Q_{gl,2} \\ Q_{gl,1} \\ Q_{gl,2} \end{bmatrix} \leq \begin{bmatrix} Q_{gl}^{\max} \\ Q_{gl,U,1} \\ Q_{gl,U,2} \end{bmatrix} \end{aligned} \quad (1)$$

where,  $Q_{l,i}$  is the liquid flowrate and  $Q_{gl,i}$  is the gas lift injection of well  $i$ . The gas injection rates are degrees of freedom  $\mathbf{u}$  of the system. All the flowrates are measured as well as the top pressures  $P_{top,1}$  and  $P_{top,2}$ . The reservoir valve openings  $vo_1$  and  $vo_2$  are considered as the system measured disturbances.  $Q_{gl}^{\max}$  and  $Q_{gl,U,i}$  are the maximum gas processing capacity of the system and maximum gas lift flowrate for each well, respectively.

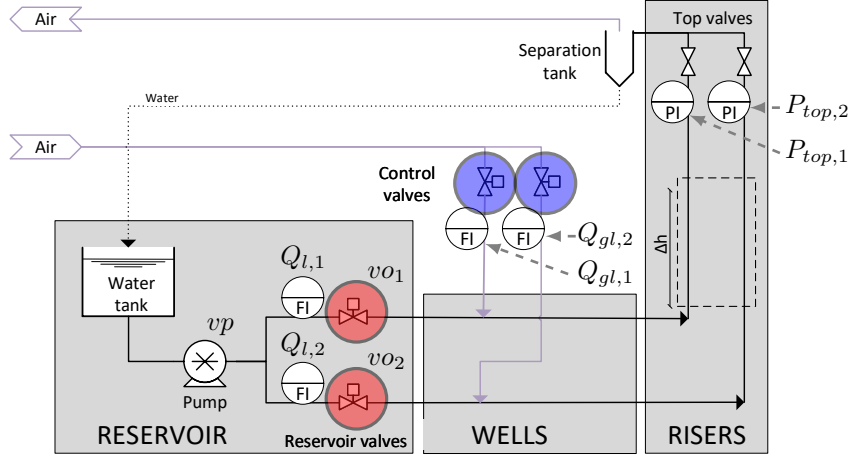


Fig. 2. Experiment schematic. The system measurements are the top pressures of well 1 and 2,  $P_{top,1}$  and  $P_{top,2}$ , and the liquid flowrates,  $Q_{l,1}$  and  $Q_{l,2}$ . The sensors are indicated by white circles. The gas lift flowrates  $Q_{gl,1}$  and  $Q_{gl,2}$ , which are the system manipulated variables, are controlled by the valves shown in blue. The reservoir valves, indicated in red, are used for representing different reservoir behaviors. Their openings,  $vo_1$  and  $vo_2$ , are considered as the system measured disturbances.  $vp$  is the pump rotation, which is kept constant in the experiments.

## 5 System model

The relationship between production flowrates  $Q_{l,i}$  and gas injection  $Q_{gl,i}$  is captured by a steady-state model (shown in the Appendix), which consists of liquid and gas mass balances, Bernoulli equation for representing the top valves, and simple relations for calculating density and pressure drop. The main simplifications are: constant temperatures, ideal gas behavior, and laminar flow.

For modeling the reservoir, we derived an empirical model that relates the reservoir outflow  $Q_{l,i}$  with the pump rotation  $vp$ , reservoir valve openings  $vo_i$  and the gas lift flowrate  $Q_{gl,i}$  of each well. This reservoir model has one adjustable parameter for each well  $\theta_{res,i}$  that, together with the top valve characteristic parameters  $\theta_{val,i}$ , are updated for representing the current plant state. This adjustable parameter set was chosen according to an identifiability analysis, which is not shown here for the sake of brevity. A dynamic model, also shown in the Appendix, is used in ROPA for parameter estimation. Both models were tested and validated against actual data, showing a good prediction capacity.

## 6 Experimental set-up

The implementation of TS-RTO and ROPA are summarized in Figures 4 and 5, shown in the next page.

In TS-RTO, the approach proposed by [Cao and Rhinehart, 1997] is used for detecting steady-state. This method calculates the variance in two distinct ways and compares them to verify if the system is at steady-state. The first variance is calculated by the difference of the measurements at the current time instant  $k$  and a filtered value of the measurement mean. The other, by the difference between the measurement at time  $k$  and at time  $k - 1$ . Next, both variances are used for computing an R-statistic. The R value is compared to a threshold, if it is smaller than  $R_{threshold}$ , the system is considered at steady-state.

For implementing ROPA, we must choose its execution period ( $\Delta T_{ROPA}$ ). It must be chosen such that relevant

process dynamics and disturbances are captured. In our implementation, ROPA executes every 10 s, which is in the same order of magnitude of the process settling time. The TS-RTO steady-state detection is also triggered at the same rate. Hence, if the steady-state wait and the stationary period detection have no influence on the performance, both methods should have similar performances.

Other important system parameters for implementing the methods are the bounds on the gas lift injection rate  $Q_{gl,U}$ , set to 4 L/min for both wells, and the maximum gas lift availability  $Q_{gl}^{max}$ , chosen as 5 L/min. The values of  $\alpha_l$  and  $\alpha_{gl}$  used for calculating the profit ( $J$  in Equation (1)) are 10 \$/L/min and 0.5 \$/sL/min. They are chosen in order to reflect that the oil selling prices are order of magnitudes larger than the gas injection costs. The initial value of the inputs is specified as  $Q_{gl,i,0} = 2.5$  sL/min for both wells. This is the naive solution, in which the total amount of available gas lift is equally divided between the two wells. Independently of the current system condition.

In order to test how both methods behave in face of disturbances, we use the reservoir valves to emulate the wells depletion (i.e. declining oil production over time). The profiles of the valve openings  $vo_1$  and  $vo_2$  are shown in Figure 3. Larger valve openings indicate that the well has a larger reservoir outflow. With time, the production capacity of both wells decreases, and we use both ROPA and TS-RTO to decide how to distribute the available gas lift between the two wells. The pump rotation  $vp$  is kept constant in all experiments.

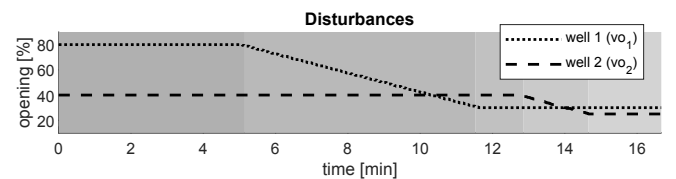


Fig. 3. System disturbances. The gray shades indicate periods in which different disturbance combinations affect the system.

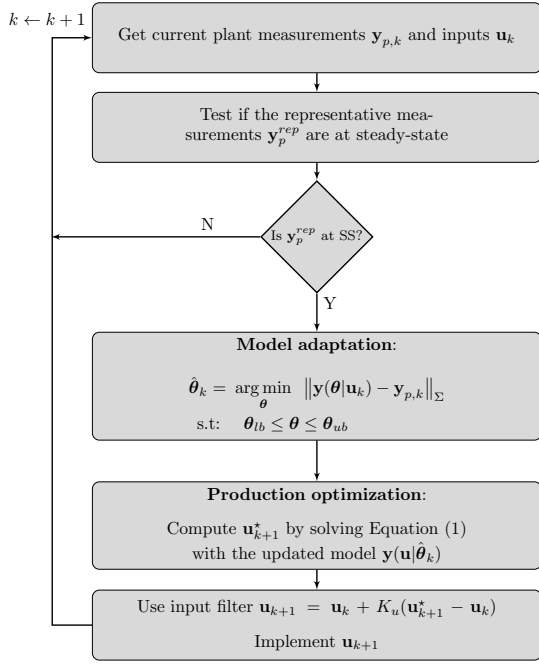


Fig. 4. TS-RTO implementation diagram. The representative measurements are a subset of the plant measurements (i.e.  $\mathbf{y}_p^{rep} \subseteq \mathbf{y}_p$ ) used for indicating whether or not the system is at steady-state.  $\mathbf{y}(\mathbf{u}|\boldsymbol{\theta})$  is a mapping that represents the solution of the steady-state model. The symbol  $\|\cdot\|_{\Sigma}$  represents the weighted norm, where the weighting matrix  $\Sigma$  is chosen as the covariance matrix of the plant measurements  $\mathbf{y}_p$ .

## 7 Experimental Results

For studying the methods, we run experiments of 16.5 minutes starting from the same operational point  $Q_{gl,i,0}$ . The results are presented in three sections. First, we show the preliminary analysis of different methods for steady-state detection. Then, we compare the results of ROPA and TS-RTO implementations in terms of: steady-state detection, parameter estimates, computed input profiles and profit. Finally, we compare the variability of the obtained cumulative profit for several different runs of both methods with the same disturbance scenario.

### 7.1 Steady-state detection

We performed an offline steady-state detection (SSD) test using the methods of Alekman [1994] (Method 1), Kelly and Hedengren [2013] (Method 2) and Cao and Rhinehart [1997] (Method 3). The representative measurements  $y_p^{rep}$  are the liquid flowrate  $Q_l$  of both wells. We used the data set from the naive solution, where  $Q_{gl,1} = Q_{gl,2} = 2.5$   $sL/min$ . We can see that different methods yield different results, as claimed by Menezes [2016]. Based on visual inspection (Figure 6), we choose to use Method 3 in the TS-RTO implementation.

### 7.2 Comparing TS-RTO and ROPA

Figure 7 shows the steady state detection results obtained during the TS-RTO experiment. The flag, shown in the

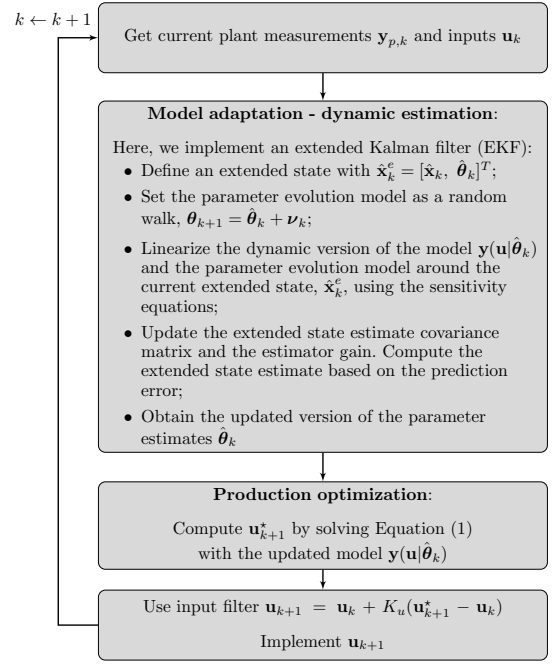


Fig. 5. ROPA implementation diagram. The process noise term  $\nu_k$  used in the parameter evolution model belongs to a sequence of independent Gaussian random values. The tuning parameters used in the EKF are not presented here for the sake of brevity.

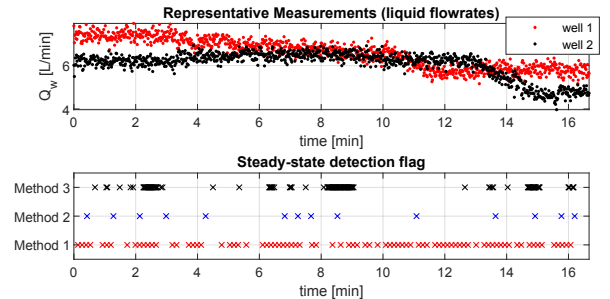


Fig. 6. Steady state detection using different methods. The  $\times$  flags of the bottom plot mark steady-state periods

bottom plot, indicates if a steady-state data period is detected (Flag = Yes) or not. As mentioned, a perfect representation of the system state (transient or steady-state) is difficult to obtain. Consequently, Method 3 tuning tends to be conservative and only a few points are indicated as steady state.

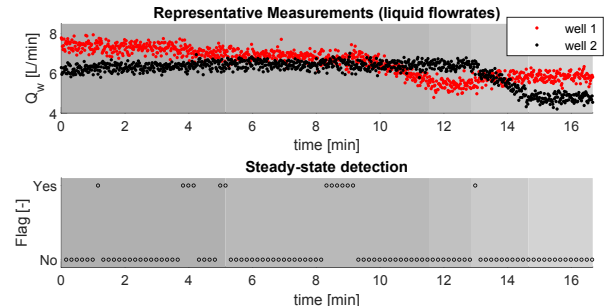


Fig. 7. Steady state detection results using the Method 3.

The parameter estimation comparison between ROPA and TS-RTO is presented in Figure 8. When the steady state is not detected, the TS-RTO parameters are graphically presented as being zero, which indicates that the system is not re-optimized (i.e. TS-RTO is not triggered). Both methods show a consistent estimation profile for the valve and reservoir parameters. However, between 8 and 10 minutes, the TS-RTO is triggered during a transient period (see the disturbance profiles in Figure 3). In this experiment, it did not affect the parameter values substantially, however this can be potentially dangerous in plant implementations.

Figure 9 shows the profile of the manipulated variable  $Q_{gl}$  values computed by each method. For the TS-RTO, the manipulated variables change only when the steady state is detected, otherwise they remain the same. On the other hand, ROPA continually updates them. Similar to the parameters, ROPA and TS-RTO manipulated variable profiles are consistent with each other. Their profiles are similar to what was expected beforehand, which can be inferred given that we know the disturbance profiles. At first, well 1 is less productive than well 2. Hence, more air is injected at well 2. As well 1 outflow decreases, between 8 and 12 minutes, more gas lift is used for increasing well 1 production. In the end of the experiment, between 14 and 16 minutes, both wells have similar outflows. Therefore, the air injection is equally shared between the wells.

Figure 10 shows a profit comparison between the approaches and the case with fixed inputs, in which the total available gas lift is equally divided between the two wells, i.e.  $Q_{gl,1} = Q_{gl,2} = 2.5 \text{ sL/min}$ . In the plots, we show the difference in percentage of the instantaneous profit between ROPA or TS-RTO and the fixed input (naive) approach (i.e.  $100(J - J_{fix})/J_{fix}$ ). Since the instantaneous profit is noisy, we show a moving average trend line (of 40 s). In general, we see that in the transient periods between 5 and 14 min, ROPA has a superior performance, as expected. On the other hand, in the initial and final periods, where the disturbances affecting the system are not changing and there is no need to re-optimize the gas lift distribution, both methods present similar performances.

In relation to the liquid production, ROPA increases the average reservoir liquid extraction by 4.9% when compared to the fixed inputs case, while the TS-RTO is less efficient, with an average production 3.9% higher than the fixed input case. Note that a productivity increase in the range of 3% – 5% without using any additional resources represents a significant advantage of both ROPA and TS-RTO over the fixed input strategy. Especially in subsea oil extraction.

### 7.3 Results variability

The economic results variability of 4 independent experiments is shown in Table 1. They indicate that ROPA has a consistent performance with higher average cumulative profit and lower variability.

## 8 Conclusion

This paper described the first actual implementation of an RTO variant called real-time optimization with persistent parameter adaptation, ROPA (also known as hybrid RTO), in which dynamic parameter estimation is included

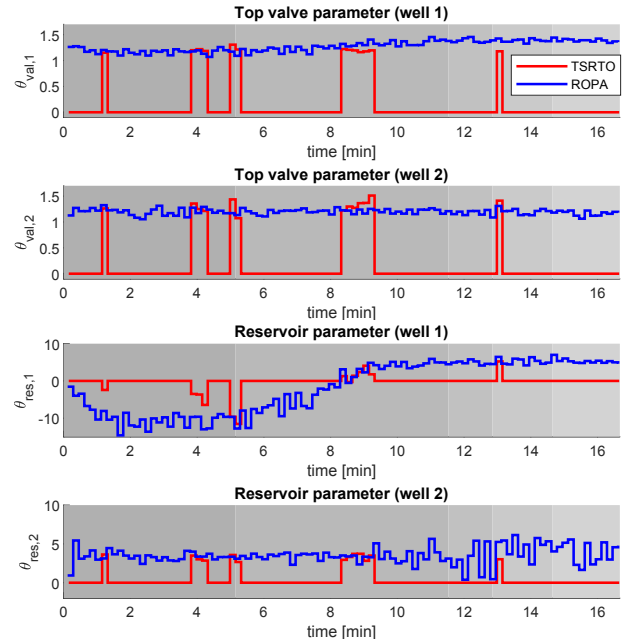


Fig. 8. Estimated parameter comparison

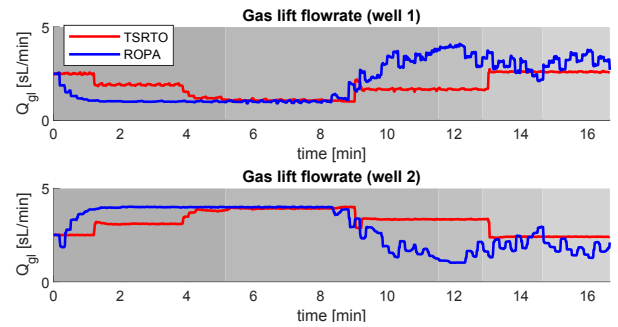


Fig. 9. Manipulated variable comparison. Input filter parameter  $K_u$  (see Figures 4 and 5) is set to 0.4.

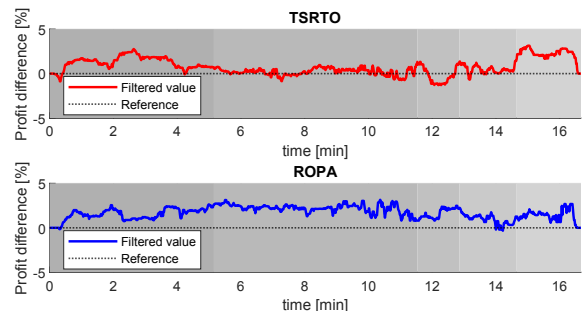


Fig. 10. Profit comparison between RTO approaches and equal gas rates for both wells. A reference line indicating no difference (0%) is added to improve readability.

Table 1. Cumulative profit obtained over 4 identical and independent experimental runs

Method	Average cumulative profit [ $10^5$ \$]	Standard deviation [ $10^5$ \$]
ROPA	1.2245	0.0208
TS-RTO	1.2112	0.0337

in the optimization cycle. We used the method for optimizing the operation of an experimental rig that emulates

a subsea oil well network. We compared its performance with the standard RTO approach, the two-step RTO. The experiments show that, by increasing the optimization frequency and decreasing the variability of the optimization results, the new method improves the overall economic performance.

## Acknowledgements

The authors acknowledge Financial Support from the Norwegian research council /Intpart, SUBPRO. Galo A. C. Le Roux acknowledges CNPq, the National Council for Scientific and Technological Development for his productivity grant (312049/2018-8).

## References

- Alekman, S. (1994). Significance tests can determine steady-state with confidence. *CONTROL for the Process Industries*, Putman Publications, Chicago, IL, 3(11), 62.
- Amara, A.B. (2017). Gas lift: past and future. In *Society of Petroleum Engineers - SPE Middle East Artificial Lift Conference and Exhibition 2016*, 420–425.
- Amrit, R., Rawlings, J.B., and Angeli, D. (2011). Economic optimization using mpc with a terminal cost. *Annual Reviews in Control*, 35(2), 178–186.
- Bhat, S.A. and Saraf, D.N. (2004). Steady-state identification, gross error detection, and data reconciliation for industrial process units. *Industrial and Engineering Chemistry Research*, 43(15), 4323–4336.
- Câmara, M.M., Quelhas, A.D., and Pinto, J.C. (2016). Performance evaluation of real industrial rto systems. *Processes*, 4(4), 44.
- Cao, S. and Rhinehart, R.R. (1997). Critical values for a steady-state identifier. *Journal of Process Control*, 7(2), 149–152.
- Chen, C.Y. and Joseph, B. (1987). On-line optimization using a two-phase approach: An application study. *Industrial and Engineering Chemistry Research*, 26(9), 1924–1930.
- Friedman, Y.Z. (1995). What’s wrong with unit closed loop optimization? *Hydrocarbon Processing*, 74(10), 107–116.
- Kelly, J.D. and Hedengren, J.D. (2013). A steady-state detection (ssd) algorithm to detect non-stationary drifts in processes. *Journal of Process Control*, 23(3), 326–331.
- Krishnamoorthy, D., Foss, B., and Skogestad, S. (2018). Steady-state real-time optimization using transient measurements. *Computers and Chemical Engineering*, 115, 34–45.
- Matias, J.O.A. and Le Roux, G.A.C. (2018). Real-time optimization with persistent parameter adaptation using online parameter estimation. *Journal of Process Control*, 68, 195–204.
- Matias, J.O.A. and Le Roux, G.A.C. (2020). Plantwide optimization via real-time optimization with persistent parameter adaptation. *Journal of Process Control*, 92, 62–78.
- Menezes, D.R.C. (2016). *Aplicação e avaliação de desempenho de um sistema de otimização em tempo real*. Master’s thesis, Universidade de São Paulo.

## A Model equations

The experimental rig model is adapted and simplified from the model shown in Krishnamoorthy et al. [2018]. The main simplifying hypothesis are: reservoir contains only liquid; the liquid and mass holdups inside the pipelines are proportional to liquid and mass flowrates; the gas is injected directly into the main pipeline (i.e. no annulus); laminar flow and ideal gas behavior are considered; and temperature is assumed constant. Since both wells have the same model, we present the model for a single well:

$$m_{tot} = m_g + m_l \quad (\text{A.1a})$$

$$m_g = m_{tot} \left( \frac{w_g}{w_g + w_l} \right) \quad (\text{A.1b})$$

$$m_l = \rho_l \left( V_{tot} - \frac{m_g}{\rho_g} \right) \quad (\text{A.1c})$$

where,  $m_{tot}$ ,  $m_l$  and  $m_g$  are the total, liquid and gas mass holdups inside riser and well pipelines.  $w_l$  and  $w_g$  are the liquid and gas flowrates.  $V_{tot}$  is the system pipelines volume.  $\rho_l$  is the density of liquid, assumed constant, and  $\rho_g$  is the gas density, which is calculated by:

$$\rho_g = P_{top} M_g / RT \quad (\text{A.2})$$

where,  $M_g$  is the air molecular weight,  $R$  the gas universal constant, and  $T$  the room temperature. The pressure at the riser top  $P_{top}$  and at the reservoir outlet  $P_{res,out}$  are:

$$P_{top} = \frac{(w_g + w_l)^2}{\theta_{val}^2 \rho_{mix}} + P_{atm} \quad (\text{A.3a})$$

$$P_{res,out} = P_{top} + \rho_{mix} g H + \frac{128 \mu_{mix} (w_g + w_l) L}{\pi \rho_{mix} D^4} \quad (\text{A.3b})$$

where,  $P_{atm}$  is the atmospheric pressure,  $\mu_{mix}$  is the mixture (liquid + gas) viscosity.  $H$ ,  $L$  and  $D$  are the height, length and diameter of the pipes.  $g$  is the gravity.  $\theta_{val}$  is the top valve flow coefficient. The mixture density  $\rho_{mix}$  is computed by:

$$\rho_{mix} = \frac{(m_g + m_l) P_{top} M_g \rho_l}{m_l P_{top} M_g + \rho_l R T m_g} \quad (\text{A.4})$$

Finally, the oil reservoir flow is given by an empirical relationship obtained using experimental data from the rig’s sensors and verified by a cross validation technique:

$$w_l = (0.01 v_o^{0.0026} - 0.9937) (1 - 0.005 w_g^2) v_{pump}^2 + \theta_{res} w_g^2 \quad (\text{A.5})$$

where,  $v_o$  and  $v_{pump}$  are the percentage of the reservoir valve opening and of the maximum pump velocity, respectively. The empirical model is identified for a given range of  $v_o$  and  $v_{pump}$ , and  $w_g$ . Every analysis in this paper is performed within this range.

**Dynamic Model:** The dynamic model is used for parameter estimation in ROPA. All the equations remain the same as in the SS model, except from mass balances:

$$\dot{m}_g = w_g - w_{g,out} \quad (\text{A.6a})$$

$$\dot{m}_l = w_l - w_{l,out} \quad (\text{A.6b})$$

$$w_{total} = w_{g,out} + w_{l,out} \quad (\text{A.6c})$$

$$w_{l,out} = x_l w_{total} \quad (\text{A.6d})$$

$$x_l = \frac{m_l}{m_l + m_g} \quad (\text{A.6e})$$

$$V_{tot} = \frac{m_l}{\rho_l} + \frac{m_g}{\rho_g} \quad (\text{A.6f})$$

where,  $w_{g,out}$  and  $w_{l,out}$  are the outlet production rate of gas and liquid.  $x_l$  is the liquid fraction in the mixture.